

Radiometric autonomous navigation for cislunar satellite Formations

Turan, E.; Speretta, S.; Gill, E.K.A.

Publication date

2022

Document Version

Final published version

Citation (APA)

Turan, E., Speretta, S., & Gill, E. K. A. (2022). *Radiometric autonomous navigation for cislunar satellite Formations*. NAVITEC 2022.

Important note

To cite this publication, please use the final published version (if applicable).
Please check the document version above.

Copyright

Other than for strictly personal use, it is not permitted to download, forward or distribute the text or part of it, without the consent of the author(s) and/or copyright holder(s), unless the work is under an open content license such as Creative Commons.

Takedown policy

Please contact us and provide details if you believe this document breaches copyrights.
We will remove access to the work immediately and investigate your claim.

RADIOMETRIC AUTONOMOUS NAVIGATION FOR CISLUNAR SATELLITE FORMATIONS

Erdem Turan⁽¹⁾, Stefano Speretta⁽²⁾, Eberhard Gill⁽³⁾

*Department of Space Engineering,
Delft University of Technology
Kluyverweg 1, 2629 HS Delft, the Netherlands
Email: ⁽¹⁾e.turan@tudelft.nl, ⁽²⁾s.speretta@tudelft.nl, ⁽³⁾E.K.A.Gill@tudelft.nl*

ABSTRACT

In this study, the application of the Linked Autonomous Interplanetary Satellite Orbit Navigation (LiAISON) method for cislunar satellite formations is investigated considering range only and range-rate only measurements. The LiAISON method provides an autonomous orbit determination solution solely using satellite-to-satellite measurements such as range and/or range-rate. This paper presents a comparison between range only and range-rate only measurements in satellite formations at cislunar space including the Earth-Moon L_1 , L_2 and Lunar orbits by presenting the results of Monte Carlo simulations and observability analysis. The results show that range observations in general provide better state estimations than range-rate observations for cislunar satellite formations in the autonomous navigation applications. However, range-rate only measurements could be an alternative to range-only measurements if range measurements are not precise and high precise range-rate measurements could be collected on-board. It has been found that range only measurements could be good enough to meet the orbit determination requirements for certain small satellite missions and allow to simplify the communication system design and reduce power usage.

INTRODUCTION

Interest in cislunar exploration with small satellites is increasing due to piggyback launch opportunities and data relay satellites in lunar orbit. In the near future, Artemis 1 will provide an opportunity for exploring cislunar space to thirteen 6U sized CubeSats which have a variety of unique mission objectives on the way to the Moon [1,2]. All these small satellite missions plan to use traditional ground-based navigation methods. However, this approach could be expensive, while the development of small satellites is expected at a low cost. Considering this and all other challenges such as on-board power limitations, autonomous navigation would be a possible solution for small satellites. Also, orbit determination requirements of certain cislunar small satellite missions [2,3] are, in general, on the order of kilometres and centimetres per second level for position and velocity, respectively. Up to now, there have been many solutions proposed in literature and one of them, the Linked Autonomous Interplanetary Satellite Orbit Navigation (LiAISON) method, uses satellite-to-satellite observations, such as range and/or range-rate to estimate absolute states when at least one of the satellites has an orbit with unique size, shape, and orientation [4-6]. The characteristics of the acceleration function determine whether solely inter-satellite range or range-rate measurements can be used to estimate the absolute and relative spacecraft states. Extensive studies have showed the capabilities of LiAISON over the past decade and cislunar and deep space missions (e.g., around asteroid) could benefit from this navigation technique [4-8].

The orbit determination performances of LiAISON depend on various factors, such as measurement precision, accuracy, frequency, observation type and others. Regarding crosslink measurements, previous studies have considered precise ranging typically less than 3 m (1σ) and 1 mm/s (1σ) for range and range-rate measurements, respectively. However, for small satellites with limited on-board power available, ranging and data-transfer are affected by the limited contact time and the ranging signal further reduces the power available for telemetry. For such cases, telemetry-based and time-derived ranging methods have been proposed [2,9,10]. However, these methods are not as precise as conventional pseudo-noise or tone-based techniques, achieving typically 150 m (1σ) ranging error at 10 kbps data-rate [10]. In the LUMIO mission, for example, the inter-satellite uplink and downlink data rates are expected to be 1 kbps and 4 kbps respectively [3]. However, it is possible to reach 10 kbps data rate with a large antenna. It is also expected that on-board Doppler measurements performed on inter-satellite links are not as accurate as measurements on ground systems due to the limited complexity of satellite communication equipment as compared to typical ground receiver. The coherent Doppler tracking also requires linear amplifiers which reduce the overall link efficiency and making it unfeasible in practical cases. This study aims at providing a realistic comparison between range only and range-rate only measurements using LiAISON at cislunar space by showing the results of the observability and Monte Carlo analysis. By doing so, the possibility of simplifying the communication system design will be investigated. In this study, first of all, a dynamical model is

provided. Orbit determination models are introduced including the observability analysis and a comparison between observation types. Thereafter, the navigation simulation setup and results are presented. Finally, conclusions are drawn.

DYNAMICAL MODEL

In this section, the orbital dynamics model used in this paper is introduced. The dynamic models used in this study are formulated based on the Circular Restricted Three-body Problem (CRTBP). The CRTBP assumes that there are two massive bodies, Earth and Moon, in orbit about their mutual barycenter as can be seen in the Fig.1. Further, the motion of P_2 relative to P_1 is assumed to be circular. The coordinate frame has its origin at the barycenter of the two bodies, P_1 and P_2 . The positive x -direction points from barycenter to P_2 . The positive y -axis is parallel to the velocity vector of P_2 and the z -axis is perpendicular to the orbital plane. The three-body gravitational parameter μ is

$$\mu = \frac{m_2}{m_1 + m_2} \quad (1)$$

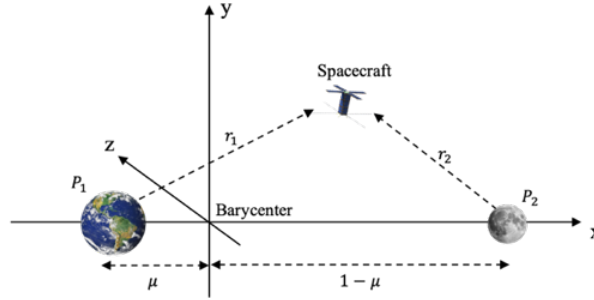


Fig. 1. Formulation for the CRTBP

where m_1 is the mass of P_1 , and m_2 is the mass of P_2 . The non-dimensional Length Unit (LU) is equal to the distance between the two primaries, so the distance along the x -axis from the origin to P_1 , is $-\mu$ LU. The Time Unit (TU) is defined such that orbital period of P_2 with respect to P_1 is 2π TU. For the Earth-Moon system, gravitational parameter μ , time conversion and length conversion parameters are 0.01215, 4.343 days/nondim time and 384747.96 km/nondim length, respectively. The equations of motion for the CRTBP [6] are

$$\ddot{x} - 2\dot{y} = x - (1 - \mu) \frac{x + \mu}{r_1^3} - \mu \frac{x + \mu - 1}{r_2^3} \quad (2)$$

$$\ddot{y} + 2\dot{x} = \left(1 - \frac{1 - \mu}{r_1^3} - \frac{\mu}{r_2^3}\right) y \quad (3)$$

$$\ddot{z} = \left(\frac{\mu - 1}{r_1^3} - \frac{\mu}{r_2^3}\right) z \quad (4)$$

where $r_1 = \sqrt{(x + \mu)^2 + y^2 + z^2}$ and $r_2 = \sqrt{(x + \mu - 1)^2 + y^2 + z^2}$.

ORBIT DETERMINATION

Autonomous crosslink navigation uses solely inter-satellite measurements. In this study, inter-satellite observations, such as range and range-rate, are collected via radiometric measurements: measuring the round-trip light time in general is based on phase measurements of a ranging signal. And, in this way, the internal clock would cause a measurement bias which can be measured along by the navigation filter or can be calibrated. The measurement model in here, referred as pseudorange, involves the geometric range, the overall clock bias, and other error sources. In the Fig.2, the concept of the two-way range measurement can be seen. Basically, Spacecraft A transmits a ranging signal at time t_1 and receives it back at time t_4 . During this measurement interval, both spacecraft move to their final relative position, so there are changes in line-of-sight direction which can be modeled as $\Delta\rho$. In the end, the geometric range can be given as:

$$R = \frac{1}{2} c(t_4 - t_1) + \Delta\rho \quad (5)$$

By assuming the speed of light is greater than the spacecraft relative velocity, i.e., $c \gg v$, and ignoring the light-time correction, the geometric range can be modeled as:

$$R = \sqrt{(\mathbf{r}_1 - \mathbf{r}_2) \cdot (\mathbf{r}_1 - \mathbf{r}_2)} = \sqrt{(x_1 - x_2)^2 + (y_1 - y_2)^2 + (z_1 - z_2)^2} \quad (6)$$

Then the pseudorange observations can be modeled as:

$$\rho = R + c(\psi_{t_4} - \psi_{t_1}) + c(\Delta_{tx} - \Delta_{rx}) + c\Delta_{trx} + \rho_{\text{noise}} \quad (7)$$

$$\rho = \sqrt{(x_1 - x_2)^2 + (y_1 - y_2)^2 + (z_1 - z_2)^2} + \rho_{\text{bias}} + \rho_{\text{noise}} \quad (8)$$

Where ψ_{t_4} and ψ_{t_1} are the on-board clock states at t_4 and t_1 respectively. Δ_{tx} and Δ_{rx} are the transponder transmit and receive line delays, respectively and Δ_{trx} is the line delay on the spacecraft transponding the ranging signal. All these terms are combined as ρ_{bias} and ρ_{noise} representing the unmodelled error sources.

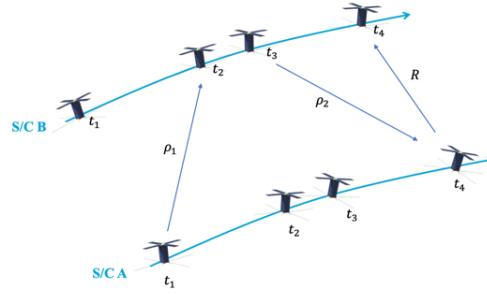


Fig. 2. Illustration of the crosslink ranging process.

Range-rate, $\dot{\rho}$, measurements can be modelled as:

$$\dot{\rho} = \frac{\boldsymbol{\rho} \cdot \dot{\boldsymbol{\rho}}}{\rho} = \frac{(x_1 - x_2)(\dot{x}_1 - \dot{x}_2) + (y_1 - y_2)(\dot{y}_1 - \dot{y}_2) + (z_1 - z_2)(\dot{z}_1 - \dot{z}_2)}{\sqrt{(x_1 - x_2)^2 + (y_1 - y_2)^2 + (z_1 - z_2)^2}} + \dot{\rho}_{\text{bias}} + \dot{\rho}_{\text{noise}} \quad (9)$$

Considering the formation formed by two spacecraft, the state vector being estimated consists of the position and velocity components of both spacecraft is given as:

$$\mathbf{X} = [x_1 \ y_1 \ z_1 \ \dot{x}_1 \ \dot{y}_1 \ \dot{z}_1 \ x_2 \ y_2 \ z_2 \ \dot{x}_2 \ \dot{y}_2 \ \dot{z}_2]^T \quad (10)$$

where the subscripts denote the spacecraft number. In this study, the Extended Kalman Filter (EKF) is adopted as a common method used in real-time navigation. The integration for the reference trajectory and the state transition matrix from t_{k-1} to t_k is based on

$$\dot{\mathbf{X}}^* = \mathbf{F}(\mathbf{X}^*, t), \quad \mathbf{X}^*(t_{k-1}) = \hat{\mathbf{X}}_{k-1} \quad (11)$$

The state transition matrix is obtained by integrating

$$\dot{\boldsymbol{\Phi}}(t, t_{k-1}) = \mathbf{A}(t)\boldsymbol{\Phi}(t, t_{k-1}), \quad \boldsymbol{\Phi}(t_{k-1}, t_{k-1}) = \mathbf{I} \quad (12)$$

where

$$\mathbf{A}(t) = \left[\frac{\partial \mathbf{F}(\mathbf{X}, t)}{\partial \mathbf{X}} \right]^* \quad (13)$$

and error covariance matrix $\bar{\mathbf{P}}$

$$\bar{\mathbf{P}}_k = \boldsymbol{\Phi}(t, t_{k-1})\mathbf{P}_{k-1}\boldsymbol{\Phi}^T(t, t_{k-1}) + \mathbf{Q} \quad (14)$$

where $\bar{\mathbf{P}}_k$ is the error covariance matrix (time updated) at time t_k . State noise compensation is introduced by adding a matrix \mathbf{Q} which can be constructed for each spacecraft as [5]:

$$\mathbf{Q} = \begin{bmatrix} \mathbf{Q}_1 & \mathbf{0} \\ \mathbf{0} & \mathbf{Q}_2 \end{bmatrix}, \quad \mathbf{Q}_m = \begin{bmatrix} \frac{\Delta t^4 \sigma_i^2}{3} & 0 & 0 & \frac{\Delta t^3 \sigma_i^2}{2} & 0 & 0 \\ 0 & \frac{\Delta t^4 \sigma_i^2}{3} & 0 & 0 & \frac{\Delta t^3 \sigma_i^2}{2} & 0 \\ 0 & 0 & \frac{\Delta t^4 \sigma_i^2}{3} & 0 & 0 & \frac{\Delta t^3 \sigma_i^2}{2} \\ \frac{\Delta t^3 \sigma_i^2}{2} & 0 & 0 & \Delta t^2 \sigma_i^2 & 0 & 0 \\ 0 & \frac{\Delta t^3 \sigma_i^2}{2} & 0 & 0 & \Delta t^2 \sigma_i^2 & 0 \\ 0 & 0 & \frac{\Delta t^3 \sigma_i^2}{2} & 0 & 0 & \Delta t^2 \sigma_i^2 \end{bmatrix}, m = 1, 2 \quad (15)$$

where Δt is time interval between measurements and σ_i is a standard deviation of unknown acceleration which has been tuned in the study until having a realistic error covariance matrix.

The observations can be related to the states using the observation-state matrix

$$\tilde{\mathbf{H}}_k = \frac{\partial \mathbf{G}(\mathbf{X}_k^*, t_k)}{\partial \mathbf{X}_k} \quad (16)$$

In this study, the crosslink range ρ and range-rate $\dot{\rho}$ are considered observations in different scenarios so that $\tilde{\mathbf{H}}_k$ is given

$$\tilde{\mathbf{H}}_k^\rho = \begin{bmatrix} \frac{\partial \rho}{\partial \mathbf{X}} \end{bmatrix}, \quad \tilde{\mathbf{H}}_k^{\dot{\rho}} = \begin{bmatrix} \frac{\partial \dot{\rho}}{\partial \mathbf{X}} \end{bmatrix} \quad (17)$$

Considering the observation errors are modelled as white Gaussian noise with standard deviation σ_ρ for range and $\sigma_{\dot{\rho}}$ for range-rate, weighting the matrix \mathbf{W}^{-1} can be used to weight observations as $\mathbf{W} = \sigma_\rho^2$ and $\mathbf{W} = \sigma_{\dot{\rho}}^2$ for range and range-rate observations respectively and the Kalman gain matrix can be calculated as:

$$\mathbf{K}_k = \bar{\mathbf{P}}_k \tilde{\mathbf{H}}_k^T [\tilde{\mathbf{H}}_k \bar{\mathbf{P}}_k \tilde{\mathbf{H}}_k^T + \mathbf{W}_k]^{-1} \quad (18)$$

Measurement and error covariance update become

$$\mathbf{x}_k = \mathbf{K}_k \mathbf{y}_k \quad (19)$$

$$\mathbf{P}_k = [\mathbf{I} - \mathbf{K}_k \tilde{\mathbf{H}}_k] \bar{\mathbf{P}}_k \quad (20)$$

$$\hat{\mathbf{X}}_k = \mathbf{X}_k^* + \mathbf{x}_k \quad (21)$$

In the end, t_k becomes t_{k-1} and the process continues till the end of the observations.

Observability

Observability analysis is a tool that can be used to relate orbit determination performances and measurement type, frequency, and accuracy. This tool provides whether the navigation parameters could be determined by the observation data, but cannot evaluate the estimation accuracy. Actually, the degree of observability can be used alone to evaluate the estimation performances. The standard approach to measure the observability is to check the observability rank condition, but this approach only provides information whether the system is observable or not. The degree of observability can be checked, for example, via the observability Gramian. For the discrete time, the time-varying observability Gramian can be written as:

$$\mathbf{N} = \sum_{k=1}^l \Phi^T(t_k, t_0) \tilde{\mathbf{H}}_k^T \tilde{\mathbf{H}}_k \Phi(t_k, t_0) \quad (22)$$

By using (22), the singular value decomposition can be performed as

$$\mathbf{N} = \mathbf{U} \mathbf{\Sigma} \mathbf{V}^T \quad (23)$$

where \mathbf{U} and \mathbf{V} are unitary matrices and $\mathbf{\Sigma}$ is a matrix of singular values. The condition number and the unobservability index can be derived from $\mathbf{\Sigma}$ in (23). The local condition number, which is the ratio of the smallest singular value to the largest singular value, and unobservability index, which is the reciprocal of the smallest singular value, are two main parameters used to measure the degree of observability or unobservability of a system. The smallest values for the unobservability index represent the states that are less difficult to be estimated from the output. If the index is large, then observation noise can have a large impact on the estimation error [11].

Observation Type Comparison

In this study, range and range-rate observations have been compared in terms of their effects on the navigation performances. Basically, a careful selection of the observation type is required which provides better orbit determination performances for the same radio measurement system. In this section, the relation between radiometric observables will be given from the measurement precision point of view. In one of the previous studies [12], a quantitative approach is given and a similar method has been used in this section. A signal-to-noise (SNR) criterion for an observable h (ρ or $\dot{\rho}$) and estimated states \mathbf{X} can be given as:

$$SNR_{h,k} = \left| \frac{1}{\sigma_h} \mathbf{H}_k \right|, \quad \mathbf{H}_k = \tilde{\mathbf{H}}_k \Phi(t_k, t_0) \quad (24)$$

Where σ_h is the noise level of the measurement h . Basically, we define the following figure of merit to compare the relative sensitivity of range and range-rate observables to estimated states, \mathbf{X} :

$$\Xi_{\mathbf{X}}^i = \frac{SNR_{\rho}}{SNR_{\dot{\rho}}} = \frac{\sigma_{\dot{\rho}}}{\sigma_{\rho}} \left| \frac{H_k^{\rho,i}}{H_k^{\dot{\rho},i}} \right| \quad (25)$$

where σ_{ρ} and $\sigma_{\dot{\rho}}$ are the noise level of the range and range-rate measurements, respectively and i represents the state component. If $\Xi_{\mathbf{X}} < 1$, it can be said that range-rate observations would become a feasible alternative to range observation for estimating \mathbf{X} . The approach given here can be considered as a ratio of the observability Gramian at each time epoch, and multiplying by a realistic relative measurement error parameter. Before making a comparison, we need to find the relation between range and range-rate observation errors, in other words the relative error parameter. As a first step, the ranging error will be defined. In case a conventional tone ranging is used for ranging operations, the following can be used to calculate the phase error on the major tone:

$$\sigma_{\rho} = \frac{\lambda}{2\pi} \sigma_r = \frac{\lambda}{2\pi} \sqrt{\frac{2B_n}{2 \frac{S}{N_0}}} \quad (26)$$

where $2B_n$, is the bi-lateral loop bandwidth, S/N_0 , the signal-to-noise ratio in dB Hz. As an example, a 30 dB Hz signal-to-noise ratio on the major tone with 0.1 Hz loop bandwidth would result in a 0.32 m ranging error. On the other hand, Doppler data noise can be expressed by the phase noise in radians and converted to range-rate noise by the following equation [13]:

$$\sigma_{\dot{\rho}} = \frac{\sqrt{2}c}{2G f_t t_c} \frac{\sigma_{\varphi}}{2\pi} \quad (27)$$

being c the speed of light, G the transponding ratio, f_t , the transmitted frequency, t_c , the integration time, σ_{φ} the phase noise in radians. As an example, for an S-band system, a 1 m ranging error would be equivalent to 0.3 mm/s range-rate

error with 1 s integration on the same ranging/Doppler unit. In brief, by using (25), it is possible to compare range only and range-rate only navigation systems in a realistic way.

NAVIGATION SIMULATIONS

In this study, various orbital configurations have been considered. These include four different orbits at the Earth-Moon L_1 and L_2 points with orbital periods between 11.81 to 12.09 days for L_1 orbiters (Jacobi constant C_j between 3.06 and 3.10) and between 13.87 to 14.35 days for L_2 orbiters (Jacobi constant C_j between 3.09 and 3.12) and a lunar orbiter with an orbital period of 0.93 days. True and estimated states are generated by using the ODE113 solver in Matlab. If not explicitly mentioned, range and range rate errors have been set to 1 m (1σ) and 0.3 mm/s (1σ) respectively. No bias is further assumed for measurements and the measurement interval has been set to $5e-3$ TU. Simulations last for one orbital period defined by the longest period in the formation. The initial covariance matrix is set to diagonal for each position and velocity component as 1 km (1σ) and 1 cm/s (1σ), respectively. The initial position and velocity in each component have an error of 500 m and 1 mm/s for both spacecraft, respectively. During the simulations, in each k th time step, the RMS error for the N th case of the Monte Carlo simulation is calculated by using the following metric:

$$RMSE_k = \sqrt{\frac{1}{N} \sum_{l=1}^N (x_{i,k} - \hat{x}_{i,k})^2} \quad (28)$$

where $x_{i,k}$ and $\hat{x}_{i,k}$ are i th components of state vector and its estimate, respectively. The 3D position and velocity errors are derived by taking the norm of the corresponding states.

Simulation Results

This section presents the simulation results. In order to not confuse the reader with all the results, at first the EML₂-Lunar orbiter scenario is presented. In this scenario, one spacecraft orbits around the EML₂ point and other one around the Moon. EML₂ Halo orbiter has a period of 14.35 days with the Jacobi energy $C_j=3.12$. Lunar orbiter has a period of 0.93 days. In Fig.3, the RMS position and velocity errors are derived for 100 Monte Carlo simulation runs via range only and range-rate only. It can be seen that during the almost 14.35 days of simulation, the range only case (blue) provides slightly better position and velocity estimations than range-rate only case (red) for both spacecraft in case 1 m (1σ) and 0.3 mm/s (1σ) measurement errors are assumed. Fluctuations in the estimations for the lunar orbiter are related to the relative geometry between satellites. It converges when the satellite approaches the periselene which is the closest point the Moon (high velocity region). Basically, the range only case provides better state estimations when satellite approaches the aposelene during the very first seven days.

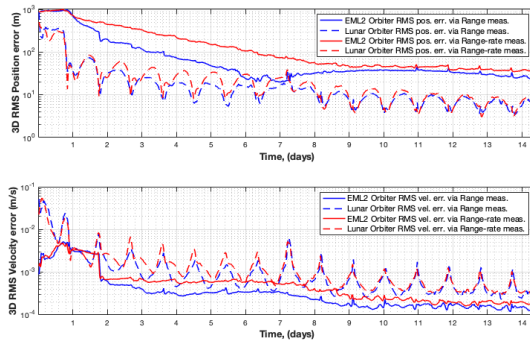


Fig. 3. EML₂-Lunar orbiter scenario, RMS position and velocity error (100 Monte Carlo runs) via range only and range-rate only.

In addition to 1 m (1σ) and 0.3 mm/s (1σ) and the EML₂-Lunar orbiter case, other geometries and measurement precisions have also been investigated. In the Fig. 4 and Fig. 5, Earth-Moon L_1 , L_2 , and Lunar orbiter RMS position errors are derived from 100 Monte Carlo simulation runs considering various range-only and range-rate only. As it can be seen, range errors vary between 1 m to 100 m and range-rate errors vary between 0.1 mm/s to 10 mm/s. In position estimation, 1 m (1σ) range error and 0.1 mm/s (1σ) range-rate error cases give similar results for the link between Lagrangian point orbiters and the Lunar orbiter. However, range data provide better position estimation for the crosslink between L_1 and

L_2 orbiters even if high error measurements are considered. On the other hand, if sub-mm/s level precision could be achieved on-board, range-rate only measurements could be an alternative to a range-only system. Basically, the sub-mm/s cases give better results than less precise range-only cases which could be from range measurements obtained with telemetry-based or time-derived methods. Also, as it can be seen from the Fig.5, high measurement errors do not bring valuable state estimation for the crosslink between Lagrangian point orbiters.

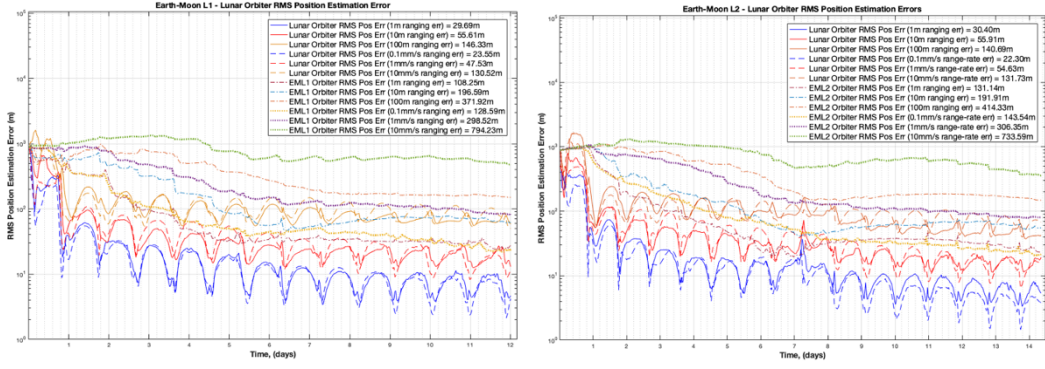


Fig. 4. (left) EML₁ – Lunar Orbiter RMS Position Error considering various range-only and range-rate only cases. (right) EML₂ – Lunar Orbiter RMS Position Error considering various range-only and range-rate only cases.

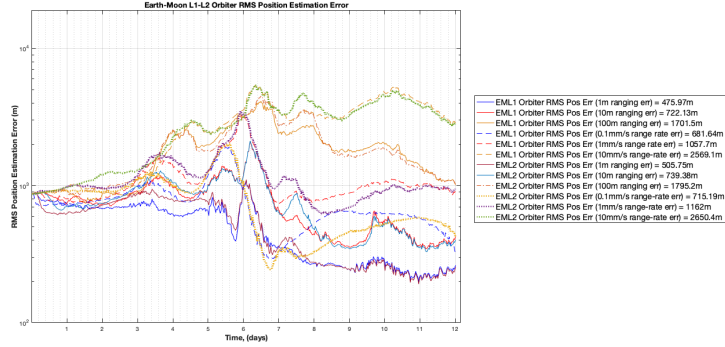


Fig. 5. Earth-Moon $L_1 - L_2$ RMS Position Error considering various range-only and range-rate only cases.

In addition to the Monte Carlo simulations, an observability analysis has been performed. Also, Ξ_x given in (25) is computed for various geometries. Table 1 presents the corresponding results: Ξ_{mean} is computed by taking the mean value of all individual Ξ_x representing the overall performance. As it can be seen, $\Xi_{\text{mean}} > 1$ for all mission scenarios with range only measurements with 1 m (1σ) error provides better state estimation than the range-rate only case with 0.3 mm/s (1σ) error. In Fig.6, the ratio Ξ for the full 12 states of the Earth-Moon L_1 -Lunar scenario can be seen.

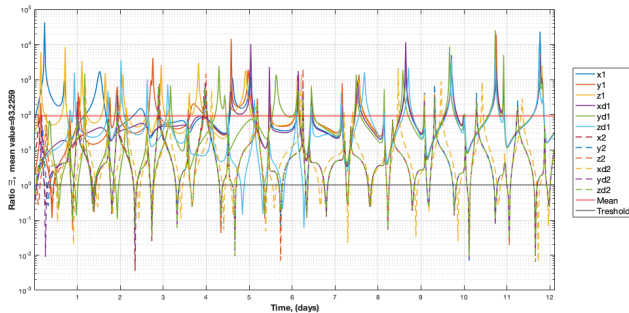


Fig. 6. Ratio Ξ_x values for the full states of the Earth-Moon L_1 -Lunar scenario

During the simulation, at certain time intervals, the ratio Ξ for certain states becomes less than unity, $\Xi < 1$, which means that the range-rate only case provides more valuable information to estimate the corresponding states than the range only case. But still, this is not sufficient for the range-rate only case to have the same overall performances with respect to the range only case, as $\Xi_{\text{mean}} = 93.22$. Also, the Earth-Moon $L_1 - L_2$ formation has higher values for both the condition number and the unobservability index than the crosslink between the Lagrangian orbiters and the Lunar orbiter, results

that are similar to the ones given in the Monte Carlo simulations presented in Fig. 3-5. In this type of application, condition number has to be less than 10^{16} for the problem to be observable [6]. As it can be seen that all the different orbital configurations give the condition number around on the order of 10^{10} . In general, for both observation types, the system is achieving better observability if halo orbits have shorter orbital periods. Lagrangian orbiters with shorter periods are in general close to the Moon and their orbital plane becomes planar, allowing to collect more information in the x-y plane.

Table 1. Ξ_{mean} , condition number, and unobservability index for various scenarios.

	EML ₁ / L ₂				EML ₁ / Lunar				EML ₂ / Lunar				
Halo Period (TU)	2.78 / 3.30	2.77 / 3.27	2.75 / 3.24	2.72 / 3.19	2.78	2.77	2.75	2.72	3.30	3.27	3.24	3.19	
Ξ_{mean} (1m/0.3mm/s)	75.87	71.29	76.32	89.11	93.22	113	79.74	69.99	64.60	63.36	83.87	71.01	
cond(N)	ρ	1.33e11	5.52e10	1.02e11	1.26e10	1.35e10	1.15e10	9.96e9	7.56e9	1.10e10	1.15e10	1.25e10	1.37e10
	$\hat{\rho}$	5.75e10	1.55e10	3.33e9	7.39e8	2.27e10	1.76e10	1.63e10	1.46e10	2.61e10	1.44e11	3.11e10	3.41e10
1/ min eig(N)	ρ	5330	4830	1.92e4	5203	373	332	295	264	201	213	233	265
	$\hat{\rho}$	487	322	164	87	0.20	0.16	0.16	0.17	0.17	0.19	0.21	0.24

CONCLUSIONS

This study investigated the application of LiAISON for cislunar satellite formations considering range only and range-rate only measurements. A comparison has been made between range only and range-rate only measurement cases for cislunar spacecraft formations at the Earth-Moon L₁, L₂ and Lunar orbits. The results from Monte Carlo simulations and observability analysis results have been presented. The results show that range observations in general provide better state estimation than range-rate observations for cislunar satellite formations performing autonomous navigation. However, range-rate only measurements could be an alternative to range-only measurements if less precise ranging methods are used (typically in the order of 100-meter error) and better than 1 mm/s range-rate precision could be collected on-board. On the other hand, even range-only measurements with high errors could be good enough to meet the orbit determination requirements for the certain cislunar small satellite missions. This would simplify the communication system design and reduce the on-board power required.

Future research might study the effects of clock bias and drift on the navigation performances. In addition, high fidelity dynamical model-based simulations are needed to compare results obtained from circular restricted three-body dynamics.

REFERENCES

- [1] D.M. McIntosh, J.D. Baker, and J.A. Matus, "The NASA CubeSat Missions Flying on Artemis-1", 2020.
- [2] E. Turan, S. Speretta, and E.Gill, "Autonomous navigation for deep space small satellites: Scientific and technological advances", *Acta Astronautica*, 193, 56-74. doi:10.1016/j.actaastro.2021.12.030.
- [3] S.Speretta, et al. "Designing the radio link for a lunar cubesat: the LUMIO case", 2021.
- [4] K. Hill, and G. H. Born, "Autonomous interplanetary orbit determination using satellite-to-satellite tracking", *Journal of Guidance, Control, and Dynamics* 30 (3) (2007) 679–686. doi:10.2514/1.24574.
- [5] K. Hill, and G. H. Born, "Autonomous Orbit Determination from Lunar Halo Orbits Using Crosslink Range", *Journal of Spacecraft and Rockets*, 45.3, 2008 doi: 10.2514/1.32316.
- [6] K. Hill, "Autonomous Navigation in Libration Point Orbits", PhD Thesis University of Colorado (2007).
- [7] J. Leonard, B. Jones, E. Villalba, and G. Born, "Absolute orbit determination and gravity field recovery for 433 eros using satellite-to-satellite tracking", in: AIAA/AAS Astrodynamics Specialist Conference, American Institute of Aeronautics and Astronautics, 2012. doi:10.2514/6.2012-4877
- [8] W. Wang, L. Shu, J. Liu, and Y. Gao, "Joint navigation performance of distant retrograde orbits and cislunar orbits via LiAISON considering dynamic and clock model errors", *Navigation* 66 (4) (2019) 781–802. doi:10.1002/navi.340.
- [9] K. Andrews, J. Hamkins, S. Shambayati, and V. Vlnrotter, "Telemetry-based ranging" 2010 *IEEE Aerospace Conference*, (pp. 1-16)
- [10] G. Iraci, and C. Gnam, "An open source radio for low cost small satellite ranging", 2018.
- [11] A.J. Krener and K.Ide, "Measures of Unobservability", 2009, doi:10.1109/CDC.2009.5400067
- [12] D. Dirkx et al. "Laser and radio tracking for planetary science missions – a comparison", *Journal of Geodesy*, 2018, 93 (11), 2405-2420., doi:10.1007/s00190-018-1171-x.
- [13] O.Montenbruck and E.Gill, "Satellite orbits: models, methods and applications" Springer Science & Business Media, 2012.